Two-fragment correlation functions for quasiprojectile source and midrapidity component at intermediate energies

Zhi-Yong He,[1,*] L. Gingras,[1] Y. Larochelle,[1] D. Ouerdane,[1,†] L. Beaulieu,[1] P. Gagné,[1,‡] Xing Qian,[1,§] R. Roy,[1] C. St-Pierre,[1] G. C. Ball,[2,‖] and D. Horn[2]

[1]*Laboratoire de Physique Nucléaire, Département de Physique, Université Laval, Québec, Canada G1K 7P4*
[2]*AECL, Chalk River Laboratories, Ontario, Canada K0J 1J0*

Two-fragment reduced-velocity correlation functions of intermediate-mass fragments emitted from midrapidity component and quasiprojectile (QP) sources formed in ^{58}Ni$+^{12}$C and ^{58}Ni$+^{197}$Au reactions at 34.5 MeV/nucleon have been studied. For the midrapidity component, they show a stronger Coulomb suppression at low relative velocities than for the QP source, suggesting a shorter emission time for it than for the QP source. Comparing the experimental correlation functions with the prediction of many-body Coulomb trajectory code, the emission times of a QP source formed in both reactions were extracted as a function of the excitation energy. The variation of emission time of the QP source with the excitation energy is independent of the reaction system. It decreases monotonically with the excitation energy in the range of $(2-6)A$ MeV from several hundred fm/c to about 100 fm/c. Above an excitation energy of $6A$ MeV, it becomes very short and saturates, suggesting that the QP source undergoes a multifragmentationlike breakup. The influence of the quasitarget fragment Coulomb interaction on QP emission time is also considered.

I. INTRODUCTION

Multifragmentation and the nuclear liquid-gas phase transition have been the subjects of numerous studies during the last decade [1,2]. The time scale of the reaction mechanisms could provide important insights into this phenomena. Information about fragment emission times can be obtained by studying the two-fragment correlation functions [3–19]. The Coulomb repulsion between emitted fragments leads to a suppression of the correlation function at small relative velocity (so-called Coulomb hole). A shorter fragment emission time results in a larger Coulomb repulsion between fragments, thus a wider Coulomb hole. The extraction of emission times is often performed by comparing experimental correlation functions with Coulomb trajectory simulation codes [13,14,20,21]. The codes consider the fragments to be emitted from the same source (one-source assumption). However, fragments in heavy ion collisions may come from various sources, such as quasiprojectile (QP), midrapidity, and quasitarget (QT) sources. To compare the experimental data with simulation results, the source selection and source identification are crucial to data analysis. Without neither impact parameter nor source selection, analysis of previous measurements could only deduce the averaged emission time scales over all sources. For example, in ^{84}Kr$+^{93}$Nb collisions at 35 MeV/nucleon, an averaged emission time of 400 fm/c was extracted for intermediate mass fragments (IMF's) detected at polar angles ranging from 7° to 35°, suggesting that a sequential binary decay occurred [3]. On the other hand, a shorter emission time scale of 200 fm/c was derived from ^{36}Ar$+^{197}$Au collisions at 35 MeV/nucleon for IMF's detected from 16° to 31° [7]. Since two-fragment correlation functions are sensitive to both emission time and source size, a careful selection of the emission source must be performed.

In this paper we report on studies of two-fragment correlation functions for quasiprojectile source and midrapidity components in ^{58}Ni$+^{12}$C and ^{58}Ni$+^{197}$Au reactions at 34.5 MeV/nucleon. After a selection of emission sources, the QP emission time is extracted by an N-body Coulomb trajectory code. The transition from long to short emission times has been deduced as a function of the QP excitation energy. We also consider influence of the QT Coulomb interaction on the QP emission time. Simulations indicate that the Coulomb interaction between QP and QT sources does not affect the extraction of the emission times, except at very short separation times.

The experimental setup is described in Sec. II. In Sec. III, data analysis and results of QP multifragment production are presented. The two-fragment correlation function for QP source and midrapidity components are discussed in Sec. IV. In Sec. V we report on the IMF emission time scale from a well-defined quasiprojectile source, extracted with an N-body Coulomb trajectory. The results of the present work are summarized in Sec. VI.

*Present address: EXFO Electro-Optical Engineering Inc., 465 Godin Avenue, Vanier, Quebec, Canada G1M 3G7.

†Present address: Niels Bohr Institute, Blegdamsvej 17, DK-2100 Copenhagen, Denmark.

‡Present address: Services Conseils Systematix, 830 Ernest - Gagnon, Québec, Qc, Canada G1S 3R3.

§Present address: Research In Motion Limited (RIM), 295 Phillip Street, Waterloo, Ontario, Canada N2L 3W8.

‖Present address: TRIUMF, 4004 Wesbrook Mall, Vancouver, B.C., Canada V6T 2A3.

II. EXPERIMENTAL SETUP

The experiment has been performed at the TASCC facility of Chalk River Laboratories, with a beam of ^{58}Ni at 34.5

MeV/nucleon incident on ^{12}C and ^{197}Au targets. The charged particles were detected in the CRL-Laval 4π array constituted by 144 detectors set in ten rings covering polar angles between $3.3°$ and $140°$. The forward four rings covering angles between $3.3°$ and $24°$ are each made of 16 plastic phoswich detectors with detection thresholds of 7.5 (27.5) MeV/nucleon for element identification of $Z=1$ (28) particles. Between $24°$ and $46°$, two rings of 16 CsI (Tl) crystals achieve isotopic resolution for $Z=1$ and 2 ions and element identification for $Z=3$ and 4 ions with thresholds ranging from 2 to 5 MeV/nucleon. The last four rings covering angles between $46°$ and $140°$ are each made of 12 CsI (Tl) crystals for isotopic resolution of $Z=1$ and 2 ions and element identification of $Z=3$ and 4 ions. Finally, three of these detectors were replaced in the third, fourth, and fifth rings by Si-Si-CsI (Tl) telescope detectors achieving isotopic resolution for $Z=1$–5 with thresholds of 2.0 (3.1) MeV/nucleon for $Z=1$ (5). The main trigger for event recording was a charged particle multiplicity of at least three particles. Details of the detectors and energy calibration can be found in Refs. [22–25].

III. DATA ANALYSIS AND RESULTS

A. Selection of impact parameter

Since the array does not have a complete angular coverage and suffers from non-negligible energy thresholds, the first step in the event-by-event analysis is to select the "well"-characterized events in which sufficient information has been obtained. It is required that a total detected charge for each event be larger than 25, i.e., 90% of the projectile charge. This selection retains the peripheral and midcentral collision events. For the ^{58}Ni+ ^{197}Au reaction, since the QT fragments with low energy cannot be detected by the array, all very central events, with no projectilelike fragments, are rejected.

The second step in the data analysis is to sort the events in terms of impact parameter. Two global variables related to the violence of the collisions have been investigated. The first one is the total charged particle multiplicity of the event (e.g., [26–28]) and the second one is the total absolute parallel momentum of the charged particles in the center-of-mass reference frame ($\Sigma|P_\parallel^{\text{c.m.}}|$), defined as

$$\Sigma|P_\parallel^{\text{c.m.}}| = \sum_{i=1}^{M} |P_{\parallel,i}^{\text{c.m.}}|, \tag{1}$$

where M is the total charged particle multiplicity of the event and $P_{\parallel,i}^{\text{c.m.}}$ is the parallel momentum of the charged particle i in the center of mass. Simulations indicate that $\Sigma|P_\parallel^{\text{c.m.}}|$ is a better parameter to extract experimental centrality for our detecting system [29].

B. Reconstruction of quasiprojectile source

To reconstruct the QP source on an event-by-event basis, a two-step statistical algorithm has been used consisting in building probability tables for the attribution of a final detected particle to the QP according to its relative velocity
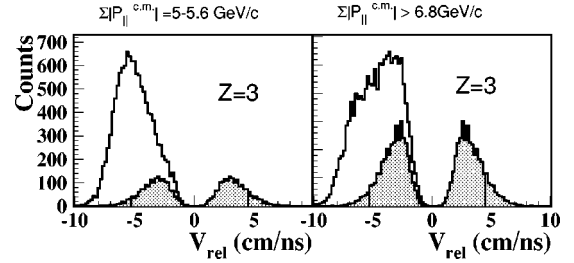

FIG. 1. Relative velocity between a $Z=3$ fragment and the QP residue of $Z=9$ for the midcentral (left panel) and peripheral (right panel) ^{58}Ni+ ^{197}Au collisions. The shaded area shows the contribution associated to the QP source.

with the evaporation residue and using these probabilities on an event-by-event basis. The events were first sorted into several groups according to the value of $\Sigma|P_\parallel^{\text{c.m.}}|$, and for each event in a group, the heaviest fragment with $Z_{res}\geq 8$ in the event was used as the QP evaporation residue. Then, particles and fragments emitted from the QP source are supposed to be distributed isotropically around this residue. The relative velocity V_{rel} is defined to be positive if the parallel velocity of the charged particle is higher than the residue parallel velocity (in the laboratory frame) and negative otherwise. As an example, Fig. 1 shows the V_{rel} spectra between $Z=3$ fragments and the QP residues of $Z=9$ emitted in ^{58}Ni+ ^{197}Au reaction for the midcentral collisions with $\Sigma|P_\parallel^{\text{c.m.}}|=5$–5.6 GeV/$c$ (left panel) and peripheral collisions with $\Sigma|P_\parallel^{\text{c.m.}}|\geq 6.8$ GeV/c (right panel). The shaded area with positive V_{rel} value in Fig. 1 represents the distribution of fragments emitted forward in the QP residue reference frame whereas the one with negative value represents its reflection on the negative V_{rel} axis. The attribution probability for forward-emitted particles is fixed at unity while the probability of backward-emitted particles is determined by dividing the reflected relative velocity spectrum with the original one. Elements of the probability tables are referenced by classes of $\Sigma|P_\parallel^{\text{c.m.}}|$, Z_{res}, Z_{cp}, and V_{rel}. The efficiency of this reconstruction method has been evaluated by its application to simulated and filtered DIT+GEMINI events where the true particle origin is known. Table I shows the rate of succesful particle attribution as a function of impact parameter and for different charges in Ni+Au system. The rate is higher than 76% for low-impact parameters and gets close to 96% for peripheral collisions. It is worthwhile noting that even in the case of particle unsuccesful attribution to the QP, the misattributed particle is statistically related to the

TABLE I. Rate (in percent) of succesful QP particle attribution for different classes of impact parameter (in fermi) and charged particles by the reconstruction method for filtered DIT+GEMINI ^{58}Ni+ ^{197}Au reactions at 34.5 MeV/nucleon simulations.

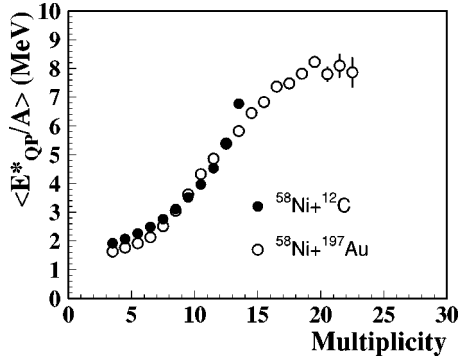| b (fm)	$Z>0$	$Z=1$	$Z=2$	$Z=3$–7	$Z=3$–14
8–10	94	89	95	89	89
6–8	88	84	88	89	91
4–6	76	73	75	81	85

FIG. 2. The averaged excitation energy per nucleon of QP source as a function of event multiplicity.

FIG. 3. The averaged reconstructed charge of the QP as a function of excitation energy per nucleon of the QP source.

QP since the statistical reconstruction is based on probalities depending on the particle relative velocity with the QP residue. Fragments in the shaded area of Fig. 1 are considered as originating from the QP source. The other backward-emitted fragments (the blank area) were attributed to the midrapidity and QT emissions. Because of the relatively high-detector-energy thresholds, these detected fragments originate mainly from the midrapidity component. All events without a QP residue were rejected from the analysis.

After the QP source was reconstructed, its excitation energy was deduced event by event by the calorimetry method [2,30–32]:

$$E^*_{QP} = \sum_{i=1}^{M_{QP}} K_i + M_n \langle K_n \rangle + Q. \tag{2}$$

M_{QP} and M_n are the charged-particle multiplicity and the QP neutron multiplicity, respectively, K_i and $\langle K_n \rangle$ the kinetic energy of each charged particle and the averaged neutron kinetic energy, and Q the mass balance of the reconstructed QP source. Since the neutrons were not detected by the array, the QP neutron multiplicity M_n was deduced from the balance of QP mass, A_{QP}, and the sum of the charged particles mass, $\Sigma_{i=1}^{M_{QP}} A_i$. The averaged neutron kinetic energy $\langle K_n \rangle$ was estimated from $\langle K_n \rangle = 2T$, where the nuclear temperature $T \sim (8 E^*_{QP}/A_{QP})^{1/2}$.

Figure 2 shows the averaged excitation energy per nucleon of the QP source as a function of the total charged-particle multiplicity for ^{58}Ni$+ ^{12}$C and ^{58}Ni$+ ^{197}$Au reactions. Monotonous increases of excitation energy with multiplicity are clearly shown for both systems. In our measurement, a maximum multiplicity of about 14 was observed for the ^{58}Ni$+ ^{12}$C reaction, corresponding to an excitation energy of 7 MeV/nucleon, while a maximum multiplicity of about 22, observed for the ^{58}Ni$+ ^{197}$Au reaction, corresponds to an averaged excitation energy of 8 MeV/nucleon. The excitation energy might be slightly overestimated in the ^{58}Ni$+ ^{12}$C case because of sources overlapping and the difficulty of disentangling them. Figure 3 shows the averaged reconstructed charge of the QP source as a function of its excitation energy, for the two reactions. Higher charges are typically reconstructed for the ^{58}Ni$+ ^{12}$C system, for the same excitation energy bin. This is a result of the overesti-

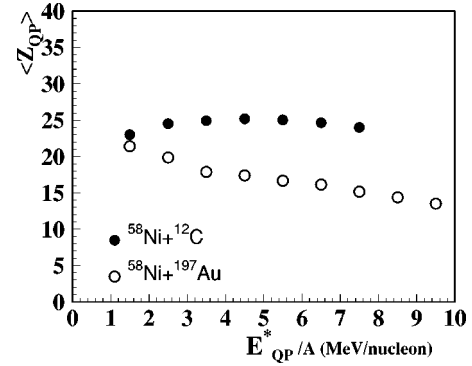mation of the QP charge in the reconstruction method because of sources overlapping, as mentioned above.

C. Multifragment production of quasiprojectile source

Before studying the two-fragment correlation functions, we examine the QP multifragment production. Figure 4 shows the probability for a given QP IMF multiplicity, N^{QP}_{IMF}, as a function of the QP excitation energy per nucleon for ^{58}Ni$+ ^{12}$C (upper panel) and ^{58}Ni$+ ^{197}$Au reactions (bottom panel), uncorrected for the detection efficiency of the array. In Fig. 4, the IMF multiplicity N^{QP}_{IMF} includes the QP evaporation residue. In both reactions, events with two IMFs emitted from the QP source begin at about $E^*_{QP}/A = 2$ MeV. Below an excitation energy of 2 MeV/nucleon, these QP source decay mainly by evaporating light particles or one fragment. At $E^*_{QP}/A \geqslant 3$ MeV, the events with three or four fragments begin to occur. The difference between these two systems is the decay production at high excitation energy. The multifragment productions in ^{58}Ni$+ ^{12}$C reaction ends at about $E^*_{QP}/A = 7$ MeV, while these in ^{58}Ni $+ ^{197}$Au reaction at about $E^*_{QP}/A = 10$ MeV.
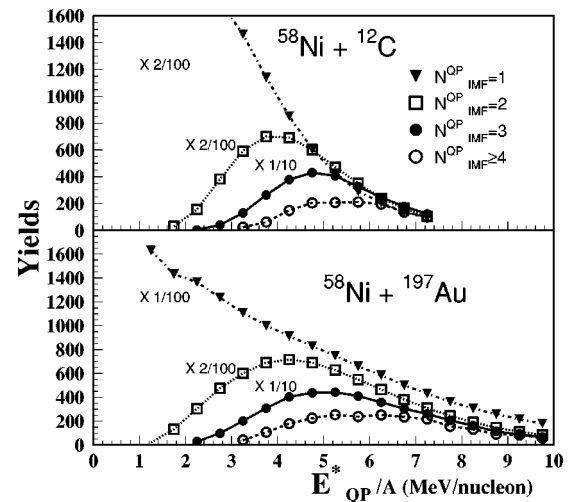

FIG. 4. Dependence on the excitation energy per nucleon of QP source E^*_{QP}/A for observing a given IMF multiplicity from QP source for ^{58}Ni$+ ^{12}$C (top panel) and ^{58}Ni$+ ^{197}$Au (bottom panel) reactions, uncorrected for the detection efficiency.
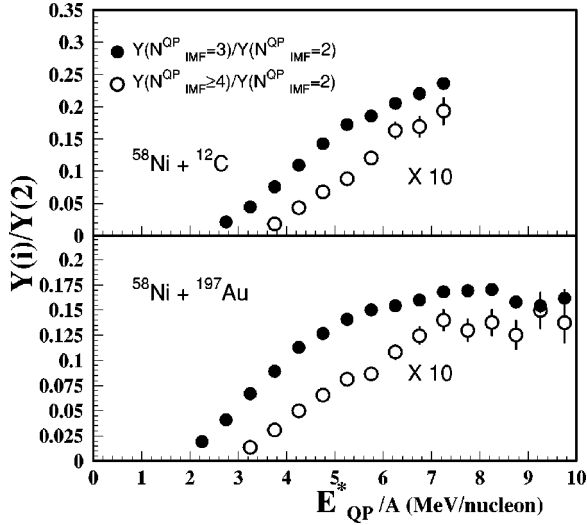
FIG. 5. Evolution of the yield ratio of the three-fragment events to two-fragment events and of the four-fragment events to two-fragment events as a function of E_{QP}^*/A for ^{58}Ni+^{12}C (top panel) and ^{58}Ni+^{197}Au reactions (bottom panel), uncorrected for the detection efficiency.

The yield ratios of the three-fragment events to two-fragment events and of the four-fragment events to two-fragment events are shown in Fig. 5, uncorrected for the detection efficiency. At a E_{QP}^*/A range between 3 and 7 MeV, the multifragment production ratio increases with E_{QP}^*/A. Above 6 MeV/nucleon, this ratio seems to saturate for ^{58}Ni+^{197}Au reaction. In the ^{58}Ni+^{12}C reaction case, the system does not reach such high excitation energies.

IV. TWO-FRAGMENT CORRELATION FUNCTIONS FOR ^{58}Ni+^{12}C AND ^{58}Ni+^{197}Au REACTIONS

To study the emission time as a function of the QP excitation energy E_{QP}^*/A, all events were sorted into several bins in terms of E_{QP}^*/A: $E_{QP}^*/A=0$-2, 2-4, 4-5, 5-6, 6-7, 7-8, and $E_{QP}^*/A\geq 8$ MeV. Emission time scales were derived from the intensity-interferometry technique which employs the two-fragment reduced-velocity correlation function defined as (e.g., [3,7,11,4])

$$1+R(V_{red})=\frac{N_{corr}(V_{red})}{N_{uncorr}(V_{red})}, \qquad (3)$$

where $N_{corr}(V_{red})$ is the observed reduced-velocity distribution $[V_{red}=|V_1-V_2|/(Z_1+Z_2)^{1/2}]$ for fragment pairs selected from the same source and the same event (coincidence distribution) and $N_{uncorr}(V_{red})$ is the reduced-velocity distribution for fragment pairs selected from mixed events (background distribution). For the results presented here, mixed events were obtained by randomly selecting each member of a fragment pair from different events with the same excitation energy range from the same source. The correlation functions are constructed according to Eq. (3), where the sum is extended over all charge combinations with $3\leq Z \leq 6$. All the fragments emitted forward and backward of the
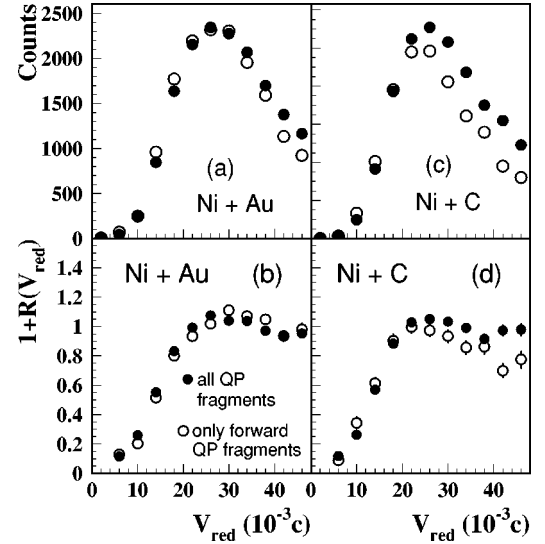

FIG. 6. Top: coincidence reduced-velocity distribution at the excitation energy bin $E_{QP}^*/A=5-6$ MeV in ^{58}Ni+^{197}Au (a) and ^{58}Ni+^{12}C reaction (c), respectively. Open and solid circles represent the results for the QP source with only forward QP fragments and with all QP fragments, respectively. The counts for the QP source with only forward QP fragments (open circles) is multiplied by 2. Bottom: two-fragment correlation function at the excitation energy bin $E_{QP}^*/A=5-6$ MeV for the QP source with only forward QP fragments (open circles) and with all QP fragments (solid circles) as a function of the reduced relative velocity V_{red}, formed in the ^{58}Ni+^{197}Au (b) and ^{58}Ni+^{12}C (d) reactions at 34.5 MeV/nucleon, respectively. Statistical error bars smaller than the size of the data points are not shown.

QP source were used for the QP correlation functions. Then all the remaining fragments which were attributed to the midrapidity emission were used to construct the midrapidity correlation functions. Sufficient statistics are achieved via this summation to allow the exploration of correlation function and emission time as a function of the QP excitation energy.

In the reconstruction of QP source, the backward fragment of QP source is obtained according to its relative velocity with the evaporation residue. The simulation indicates that about (11–19)% of these fragments may not come from the QP source (Table I). To remove this contamination, the correlation function of the QP source can be constructed with the fragments only emitted forward from the QP source. In Fig. 6, we compare the experimental correlation functions for the QP source with only forward QP fragments (open circles) and with all QP fragments (solid circles) at the excitation energy bin $E_{QP}^*/A=5-6$ MeV as a function of the reduced relative velocity V_{red}, formed in ^{58}Ni+^{197}Au (b) and ^{58}Ni+^{12}C reactions (d) at 34.5 MeV/nucleon, respectively. Figures 6(a) and 6(c) show the coincidence reduced-velocity distribution [i.e., $N_{corr}(V_{red})$ in Eq. (3)] in the ^{58}Ni+^{197}Au and ^{58}Ni+^{12}C reactions, respectively. For the ^{58}Ni+^{197}Au reaction, as shown in Figs. 6(a) and 6(b), the same two-fragment coincidence spectra and correlation functions are obtained with both methods, indicating that the correlation function constructed with the forward and backward
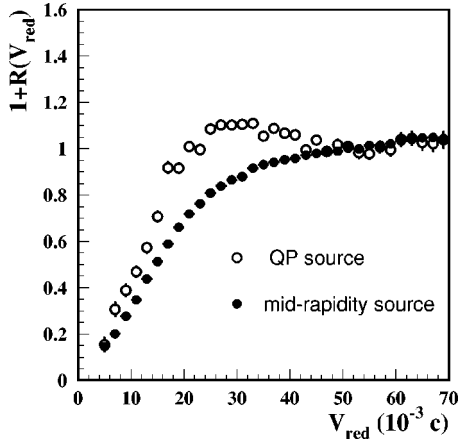
FIG. 7. Two-fragment correlation function, integrated over all fragment pairs with element $3 \leqslant Z \leqslant 6$, for $^{58}\text{Ni} + ^{197}\text{Au}$ reaction at $E/A = 34.5$ MeV. Open and solid circles represent the results for fragments from a quasiprojectile (QP) source and a midrapidity source, respectively. Statistical error bars smaller than the size of the data points are not shown.

FIG. 8. Two-fragment correlation functions, integrated over all fragment pairs with element $3 \leqslant Z \leqslant 6$, for the midrapidity component in the $^{58}\text{Ni} + ^{197}\text{Au}$ reaction for three ranges of the excitation energy of the QP source. Statistical error bars smaller than the size of the data points are not shown.

fragments exhibits the same characteristics as the correlation function made with forward fragments only. For $^{58}\text{Ni} + ^{12}\text{C}$ reaction, as shown in Fig. 6(c), the two-fragment coincidence spectra constructed with both forward and backward fragments show the same characteristics as that with only forward fragments at small reduced relative velocities ($V_{red} \leqslant 0.02c$). The coincidence spectra constructed with forward fragments only has lost a lot of events at large reduced relative velocities, as compared with that constructed with all fragments. However, these events at large V_{red} do not affect the characteristics of the correlation function and the extraction of emission time. In the following analysis, we use all QP fragments for the construction of QP correlation function to achieve enough statistics.

A. $^{58}\text{Ni} + ^{197}\text{Au}$ reaction

In Fig. 7 we compare the experimental correlation functions as a function of the reduced relative velocity V_{red} for the midrapidity component, defined as *not* coming from the QP (solid circles) and for the QP source (open circles), formed in the $^{58}\text{Ni} + ^{197}\text{Au}$ reaction at 34.5 MeV/nucleon. These correlation functions exhibit pronounced deficits or yield suppressions at low V_{red} which are manifestations of the repulsive final-state Coulomb interaction between emitted fragments. A compact source that quickly emits fragments results in a larger Coulomb interaction between the emitted fragments than a larger source emitting particles more slowly. The two-fragment correlation function of midrapidity component shows a stronger Coulomb suppression at low V_{red} than the QP source, suggesting a shorter emission time for the midrapidity component than the QP source. Figure 8 shows the correlation functions for fragment pairs selected from the midrapidity component for QP excitation energies $E_{QP}^{*}/A = 0–2$ MeV (solid squares), 5–6 MeV (open circles), and 7–8 MeV (solid circles), respectively. Coulomb suppression at low V_{red} for the midrapidity
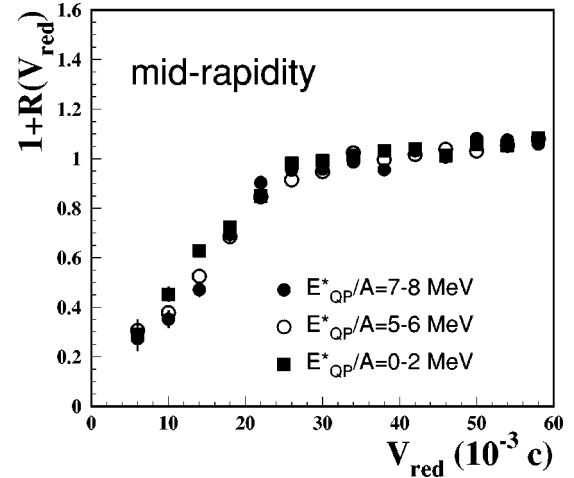
component changes very slightly with E_{QP}^{*}/A, indicating that the emission time of the midrapidity component is independent of the QP excitation energy.

The top panel of Fig. 9 shows the correlation functions for fragment pairs selected from the QP source formed in $^{58}\text{Ni} + ^{197}\text{Au}$ reaction for QP excitation energy bins $E_{QP}^{*}/A = 2–4$ MeV (solid squares), 5–6 MeV (open circles), and 7–8 MeV (solid circles). Since few events with two IMFs from the QP source were observed at an excitation energy below 2 MeV/nucleon (see Fig. 4), we do not construct the corresponding correlation functions. In contrast with the midrapidity component, the yield suppression at low V_{red} in the QP correlation function due to the Coulomb interaction
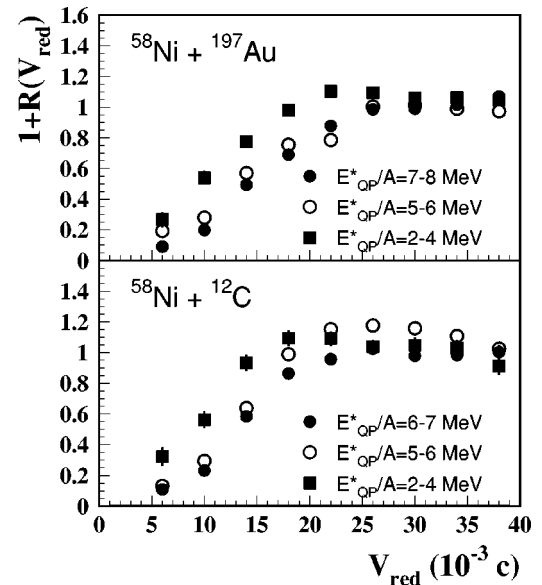

FIG. 9. Two-fragment correlation functions for the QP source formed in the $^{58}\text{Ni} + ^{197}\text{Au}$ (top panel) and $^{58}\text{Ni} + ^{12}\text{C}$ (bottom panel) reactions for some excitation energy ranges of QP source.

between fragments increases obviously with E_{QP}^*/A, indicating that the emission time of the QP source decreases with increasing excitation energy.

B. ^{58}Ni + ^{12}C reaction

The bottom panel of Fig. 9 shows the correlation function for fragment pairs selected from QP source formed in ^{58}Ni + ^{12}C reaction for an excitation energy range E_{QP}^*/A = 2–4 MeV (solid squares), 5–6 MeV (open circles) and 6–7 MeV (solid circles). Since few events with two QP IMFs are observed at neither $E_{QP}^*/A < 2$ MeV nor $E_{QP}^*/A > 6$ MeV in the ^{58}Ni + ^{12}C reaction (see Fig. 4), the QP correlation functions are constructed only for a E_{QP}^*/A range from 2 to 7 MeV and are divided into four bins: E_{QP}^*/A = 2–4, 4–5, 5–6, 6–7 MeV. As in the ^{58}Ni + ^{197}Au reaction, the Coulomb suppression at low V_{red} in the correlation function for the QP source formed in ^{58}Ni + ^{12}C reaction increases obviously with E_{QP}^*/A. The increase of the Coulomb suppression is large between 2 and 5 MeV, but then drops to become negligible at higher excitation energies. The QP emission time as a function of the excitation energy will be studied in detail in the next section.

To study the correlation function of the midrapidity component in the ^{58}Ni + ^{12}C reaction, we accumulate all the events with two IMFs. Since the ^{58}Ni + ^{12}C reaction is a reverse kinetic system with a light target of $Z = 6$, one of the two correlated fragments might come from the target, the another from the midrapidity velocity source. For the ^{58}Ni + ^{197}Au reaction, sufficient statistics were achieved for the midrapidity component at all excitation energy bins. However, for the ^{58}Ni + ^{12}C reaction, sufficient statistics is achieved only at low excitation energies.

As in the ^{58}Ni + ^{197}Au reaction, the Coulomb suppression at low V_{red} for the midrapidity component in ^{58}Ni + ^{12}C reaction changes very slightly with E_{QP}^*/A. In Fig. 10 we compare the experimental correlation functions for the midrapidity component and QP source formed in the ^{58}Ni + ^{12}C reaction at 34.5 MeV/nucleon. At low excitation energy E_{QP}^*/A = 2–4 MeV, the two-fragment correlation function of midrapidity component shows a stronger Coulomb suppression at low V_{red} than the QP source. However, at E_{QP}^*/A = 5–6 MeV, there are few differences between the two correlation functions.

V. EMISSION TIME SCALE OF QUASIPROJECTILE SOURCE

The QP emission time scale at various excitation energies is extracted by comparing the experimental two-fragment correlation functions with simulations of the many-body Coulomb trajectory code of Glasmacher *et al.* [2,13,14]. This code considers the fragments to be emitted from the surface of the source. The fragment emission times t_i were assumed to have the probability distribution $P(t) \sim e^{-t/\tau}$, where τ is the emission time of the source. Recoil velocity and mass conservation of the source are taken into account for each subsequent emission. The centers of the fragments were ini-
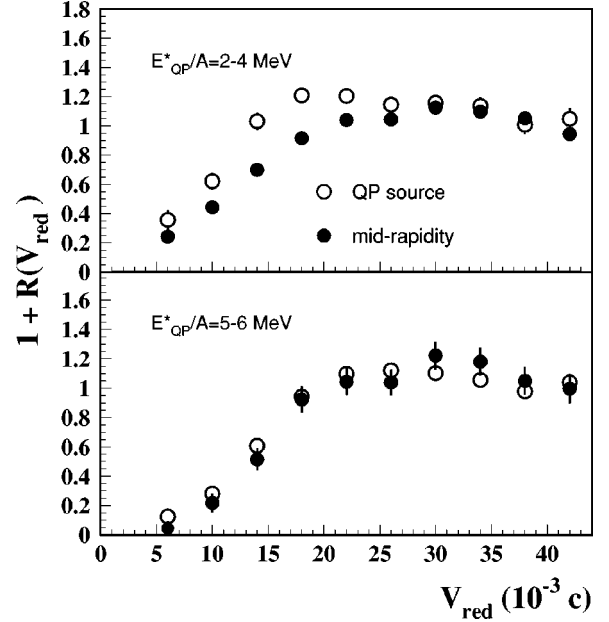

FIG. 10. Two-fragment correlation functions for the midrapidity component and QP source formed in the ^{58}Ni + ^{12}C reaction at two excitation energy bins E_{QP}^*/A = 2–4 MeV (top panel) and 5–6 MeV (bottom panel).

tially placed at a distance of $R = R_S + R_{IMF} = rA_S^{1/3} + 1.2A_{IMF}^{1/3}$ from the center of the source, where r, A, and A_{IMF} are nuclear radius parameter, mass of the source, and mass of the fragment, respectively. The mass, charge, and energy of fragments were generated by randomly sampling the experimental yield distributions. After each emission, charge and mass of the emitted fragments were subtracted from the source. Because the charge, mass, and velocity of the starting source as well as the final residue are known from the experiments, no empirical adjustment of these quantities is possible. Therefore, there are only two adjustable parameters in the simulation: the emission time τ and the nuclear radius parameter r (or nuclear density ρ). To better extract the emission time τ, we tried a large range of source sizes, from $r = 1.54$ fm to $r = 2.22$ fm. This range corresponds to a nuclear density range from $\rho = \rho_0/2$ to $\rho_0/6$ ($\rho_0/1.44$ to $\rho_0/4$) using $r_0 = 1.22$ fm (1.44 fm) as a normal nuclear radius parameter. To compare with the experimental data, the calculations are filtered by the acceptance of the experimental apparatus. We only perform these simulations for a well-defined QP source to extract their emission time. Since the source of midrapidity component is not fully known, we do not perform these simulations for the later case.

Figure 11 shows fits to the correlation functions of QP source formed in ^{58}Ni + ^{12}C reaction for three bins in excitation energy for a range of nuclear density ρ and emission time τ that yield minimum χ-square values. Figures 11(a) and 11(b) show correlation functions for the two lower excitation energy bins of E_{QP}^*/A = 2–4 MeV and 4–5 MeV, respectively. For the lowest E_{QP}^*/A bin, a long emission time of about 600 fm/c was extracted, indicating that the QP source emits fragments by sequential binary disassembly. As
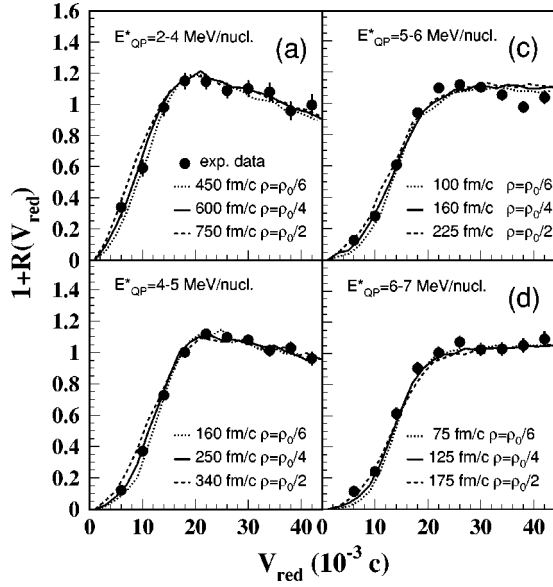
FIG. 11. Two-fragment correlation functions for the QP source formed in ^{58}Ni+ ^{12}C reactions at four excitation energy bins $E^*_{QP}/A = 2$–4, 4–5, 5–6, and 6–7 MeV. The solid, dashed, and dot-dashed curves represent calculated correlation functions of a Coulomb trajectory calculation for fit parameters indicated in the figure. Statistical errors are shown as vertical bars.

FIG. 12. Emission time of QP source as a function of excitation energy of QP source for ^{58}Ni+ ^{12}C (top) and ^{58}Ni+ ^{197}Au (bottom) reactions at 34.5 MeV/nucleon. Open and solid circles represent the emission time with only forward QP fragments and with all QP fragments, respectively.

the excitation energy is raised from 2 MeV/nucleon to 5 MeV/nucleon, the emission time scale decreases monotonically from 600 fm/c to 250 fm/c. Figures 11(c) and 11(d) show correlation functions for the highest bin of $E^*_{QP}/A = 5$–6 and 6–7 MeV. Here, the emission time of the QP source becomes very short (~ 100 fm/c) and nearly independent of the excitation energy. The emission times of the QP source formed in ^{58}Ni+ ^{12}C reaction at various excitation energies are summarized in the top panel of Fig. 12 (solid circles). Open circles in the top panel of Fig. 12 represent the results for the QP source with only forward QP fragments. The error bars shown in the figure reflect the space-time ambiguity of the correlation functions. The shaded band shows the range of space-time values for which a consistent fit to all of the observations is achieved. A clear evolution of emission time with excitation energy is observed.

To compare the emission times for QP sources formed in two different systems, the bottom panel of Fig. 12 presents previous results on the emission times for the QP source formed in the ^{58}Ni+ ^{197}Au reaction as a function of the excitation energy [18]. Open and solid circles represent the emission time of the QP source with only forward QP fragments and with all QP fragments, respectively. At low excitation energy $E^*_{QP}/A = 2$–4 MeV in the ^{58}Ni+ ^{197}Au reaction, not enough statistics is achieved to extract the emission time. It is observed from Fig. 12 that the deduced emission times are the same, within experimental errors, for both situations, all fragments included or only those emitted forward of the QP. That gives more support to the QP statistical reconstruction method. As in the ^{58}Ni+ ^{12}C reaction, the QP emission time in the ^{58}Ni+ ^{197}Au reaction decreases with excitation energy, from more than 500 fm/c at E^*_{QP}/A

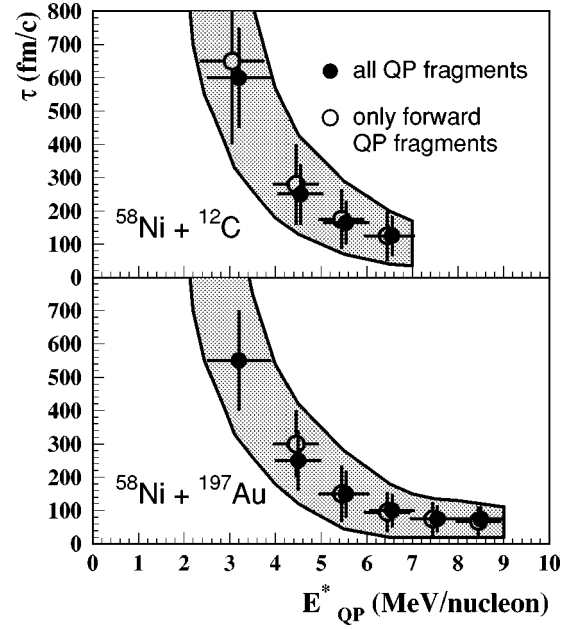$= 2$ MeV to 100 fm/c at $E^*_{QP}/A = 6$ MeV. This suggests that the QP emission time decreases with the excitation energy, independently of the reaction system. In Fig. 12, the emission time for both systems becomes very short and goes toward saturation above an excitation energy of 6 MeV. For these events with three and more fragments from the QP (see Fig. 4), such a short emission time is interpreted as a evidence of the multifragmentation process for QP breakup.

In our simulations, only the Coulomb interactions between the QP source and fragments is considered. Since fragments in heavy ion collisions may come from various sources, such as QT, midrapidity, and QP sources, the fragments from the midrapidity component and the QT source may affect the extracted QP emission time. To estimate the influence of the Coulomb interaction between QP fragments and QT fragments on the QP source emission time, we added heavy QT fragments in the many-body Coulomb trajectory simulations of the QP source. For simplicity, all fragments from the midrapidity component and the QT source are considered as a heavy fragment with a charge $Z_{QT} = Z_{system} - Z_{QP}$, where Z_{system} and Z_{QP} are the charges of the reaction system and the QP source, respectively. For a given charge number Z_{QT}, the mass number A_{QT} of the QT fragment is chosen as that of the most abundant isotope and its radius to be $R_{QT} = 1.2(A_{QT})^{1/3}$. Since the experimental QP velocity is known, the velocity of heavy QT fragments, V_{QT}, can be deduced from momentum conservation. In the simulation, the separation time between QT and QP sources, τ_S, which is defined as the separation time interval between the QT and the QP before the QP decays, is used as an adjustable parameter. So when the QP source begins to decay, the center
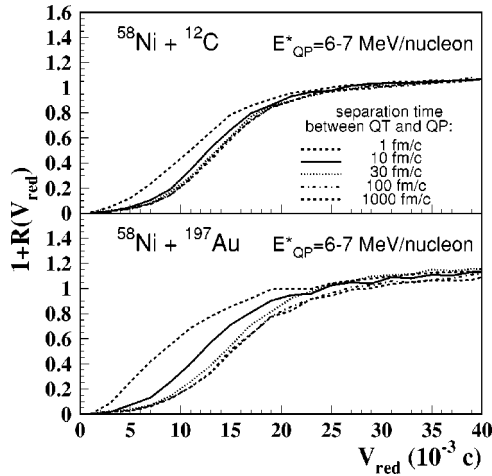
FIG. 13. QT source influence on the QP fragment emission time. The QP source emission times are fixed to 100 fm/c for ^{58}Ni $+ ^{12}$C (top) and 75 fm/c for ^{58}Ni$+ ^{197}$Au (bottom) reactions. The QP source emission times are fixed to 125 fm/c for Ni+C (top) and 100 fm/c for Ni+Au (bottom) reactions.

of the QT fragment is placed at a distance of $R = V^*_{QT}\tau_{QT}$ from the QP center.

Figure 13 shows the QP correlation functions for the bin $E^*_{QP}/A = 6-7$ MeV with separation time τ_S between the QT and QP of 1, 10, 30, 100, and 1000 fm/c. The top panel of Fig. 13 shows the correlation functions for the ^{58}Ni$+ ^{12}$C reaction. The QP fragment emission time and the QP source nuclear density are fixed to 100 fm/c and $\rho = \rho_0/4$. The correlation functions change significantly only when τ_S becomes very short ($\leqslant 10$ fm/c). For a long τ_S value, they change very slightly, due to the large relative velocity between QP and QT sources. A τ_S value of 50 fm/c results in a separation between the QP and QT of around 10 fm, twice the QP radius, before QP fragments are emitted. The bottom panel of Fig. 13 shows the correlation functions with various τ_S values for the ^{58}Ni$+ ^{197}$Au reaction. The QP fragment emission time and the QP source nuclear density are fixed to 75 fm/c and $\rho = \rho_0/4$. As in the ^{58}Ni$+ ^{12}$C reaction, the correlation function changes with τ_S only when $\tau_S \leqslant 10$ fm/c. Since the separation time between QP and QT sources should be longer than 10 fm/c, the result in Fig. 13 suggests that the QT influence can be omitted in our simulation of the QP source emission times.

VI. CONCLUSION

Two-fragment reduced-velocity correlation functions of the intermediate-mass fragments emitted from midrapidity component and quasiprojectile source formed in ^{58}Ni$+ ^{12}$C and ^{58}Ni$+ ^{197}$Au reactions at 34.5 MeV/nucleon have been studied. In both reactions, the two-fragment correlation functions for the midrapidity component show a stronger Coulomb suppression at low V_{red} than for the QP source, suggesting a shorter emission time for the midrapidity component than the QP source. In the ^{58}Ni$+ ^{197}$Au reaction, this Coulomb suppression at low V_{red} for the midrapidity component changes very slightly with E^*_{QP}/A, indicating that their emission time is independent of the excitation energy of QP source.

For the QP source, the two-fragment production is negligible at low excitation energies $E^*_{QP}/A \leqslant 2$ MeV, while the multifragment production starts at $E^*_{QP}/A \geqslant 3$ MeV, for both reactions. Above $E^*_{QP}/A \geqslant 6$ MeV, the multifragment production seems to present a saturation in the ^{58}Ni$+ ^{197}$Au reaction, while there is little multifragment production in the ^{58}Ni$+ ^{12}$C reaction. Comparing the experimental correlation functions with the many-body Coulomb trajectory code, the QP emission times were extracted as a function of the QP excitation energy. The QP emission time changes with the excitation energy, independently of the reaction system. It decreases monotonically with the excitation energy in the range of $(2-6)A$ MeV from several hundreds fm/c to about 100 fm/c. Above an excitation energy of $6A$ MeV, it becomes very short and saturates, suggesting that QP breakup follows the multifragmentation scenario. We also consider the influence of the Coulomb interaction of the QT source on the QP source emission time. Simulations indicate that the Coulomb interaction between QP and QT sources does not affect the extracted emission time, except at a very short separation time between the QP and the QT.

[1] L.G. Moretto and G.J. Wozniak, Annu. Rev. Nucl. Part. Sci. **43**, 379 (1993), and references therein; W.G. Lynch, *ibid.* **37**, 493 (1987), and references therein.

[2] L. Beaulieu *et al.*, Phys. Rev. Lett. **84**, 5971 (2000).

[3] E. Bauge *et al.*, Phys. Rev. Lett. **70**, 3705 (1993).

[4] D.R. Bowman *et al.*, Phys. Rev. Lett. **70**, 3534 (1993).

[5] D.R. Bowman *et al.*, Phys. Rev. C **52**, 818 (1995).

[6] Y.D. Kim *et al.*, Phys. Rev. Lett. **67**, 14 (1991).

[7] Y.D. Kim *et al.*, Phys. Rev. C **45**, 338 (1992); **45**, 387 (1992).

[8] T.C. Sangster *et al.*, Phys. Rev. C **47**, R2457 (1993).

[9] T.C. Sangster *et al.*, Phys. Rev. C **51**, 1280 (1995).

[10] E. Cornell *et al.*, Phys. Rev. Lett. **75**, 1475 (1995).

[11] D. Fox *et al.*, Phys. Rev. C **47**, R421 (1993).

[12] D. Fox *et al.*, Phys. Rev. C **50**, 2424 (1994).

[13] T. Glasmacher *et al.*, Phys. Rev. C **50**, 952 (1994).

[14] R. Popescu *et al.*, Phys. Rev. C **58**, 270 (1998).

[15] G. Wang *et al.*, Phys. Rev. C **60**, 014603 (1999).

[16] Zhi Yong He *et al.*, Nucl. Phys. **A620**, 214 (1997).

[17] Zhi Yong He *et al.*, Phys. Rev. C **57**, 1824 (1998).

[18] Zhi Yong He *et al.*, Phys. Rev. C **63**, 011601(R) (2000).

[19] D. Durand, Nucl. Phys. **A630**, 52c (1998), and references therein.

[20] A. Elmaani *et al.*, Nucl. Instrum. Methods Phys. Res. A **313**, 401 (1992).

[21] A. Elmaani *et al.*, Phys. Rev. C **49**, 284 (1994).

[22] Y. Larochelle *et al.*, Nucl. Instrum. Methods Phys. Res. A **348**, 167 (1994).

[23] C. Pruneau *et al.*, Nucl. Instrum. Methods Phys. Res. A **297**, 404 (1990).

[24] D. Horn *et al.*, Nucl. Instrum. Methods Phys. Res. A **320**, 273 (1992).

[25] D. Fox *et al.*, Nucl. Instrum. Methods Phys. Res. A **374**, 63 (1996).

[26] R. Stock, Phys. Rep. **135**, 259 (1986).

[27] M.B. Tsang *et al.*, Phys. Rev. C **40**, 1685 (1989).

[28] J. Péter *et al.*, Nucl. Phys. **A519**, 611 (1990).

[29] L. Gingras *et al.*, Proceedings of the XXXVI International Winter Meeting on Nuclear Physics, Bormio, Italy, 1998, p. 365.

[30] J. Pochodzalla *et al.*, Phys. Rev. Lett. **75**, 1040 (1995).

[31] Y.G. Ma *et al.*, Phys. Lett. B **390**, 41 (1997).

[32] M. D'Agostino *et al.*, Phys. Lett. B **473**, 219 (2000).